Atmos. Meas. Tech. Discuss., 3, 3455–3487, 2010
www.atmos-meas-tech-discuss.net/3/3455/2010/
doi:10.5194/amtd-3-3455-2010

Atmospheric Measurement Techniques Discussions

Fine-scale turbulence soundings in the stratosphere with the new balloon-borne instrument LITOS

A. Theuerkauf, M. Gerding, and F.-J. Lübken

Leibniz-Institute of Atmospheric Physics at the Rostock University, Kühlungsborn, Germany

Received: 11 July 2010 – Accepted: 20 July 2010 – Published: 18 August 2010

Correspondence to: A. Theuerkauf (theuerkauf@iap-kborn.de)

Published by Copernicus Publications on behalf of the European Geosciences Union.

Abstract

We have developed a new compact balloon payload called LITOS (Leibniz-Institute Turbulence Observations in the Stratosphere) for high resolution wind turbulence soundings up to 35 km altitude. The wind measurements are performed applying a constant temperature anemometer (CTA) with a vertical resolution of ~2.5 mm, i.e. 2 kHz sampling rate at 5 m/s ascent speed. Thereby, for the first time, it is possible to study the entire turbulence spectrum down to the viscous subrange in the stratosphere. Including telemetry, housekeeping, batteries and recovery unit the payload weighs less than 5 kg and can be launched at any radiosonde station. Since autumn 2007 LITOS has been successfully launched several times from the Leibniz-Institute of Atmospheric Physics (IAP) in Kühlungsborn, Germany (54° N, 12° E). Two additional soundings were carried out in 2008 and 2009 at Kiruna, Sweden (67° N, 21° E) as part of the BEXUS program (Balloon-borne EXperiments for University Students). We describe here the basic principle of CTA measurements and prove the validity of this method in the stratosphere. First case studies allow a clear distinction between non-turbulent layers and turbulent layers with a thickness of some tens of meters. Since our measurements cover the transition between the inertial and viscous subrange, energy dissipation rates can be calculated with high reliability.

1 Introduction

Gravity waves and turbulence play a crucial role in the understanding of the energy budget, momentum transfer and trace gas distribution in the atmosphere. Breaking gravity waves produce turbulent structures in temperature and wind fields as well as generate new gravity waves at the same time. Typically the stratosphere is statically stable and well stratified, due to its small negative or even positive temperature gradient. Nevertheless gravity waves can induce instability leading to wave breaking and turbulence.

AMTD
3, 3455–3487, 2010

Stratospheric turbulence is assumed to be weak on average compared to, for instance, mesospheric turbulence (e.g., Lübken, 1992; Hocking, 1990). But breaking gravity waves in the stratosphere potentially modify the energy transfer from the troposphere into the mesosphere. Observations show that the vertical growth rate of gravity waves in the stratosphere is smaller than expected for undisturbed propagation (e.g., Rauthe et al., 2008). This implies that some of the wave energy is deposited in the stratosphere. Therefore this energy can not contribute to the mesospheric energy budget. Moreover stratospheric turbulence is a potentially important process in the vertical mixing of trace species (e.g., Lilly et al., 1974).

Turbulence in the stratosphere appears on scales between some millimeters and several meters. Previous observations have shown that it occurs in thin isolated layers extending some ten or hundred meters in the vertical and some hundred kilometers in the horizontal (e.g., Barat, 1982; Sato and Woodman, 1982). The turbulent regions are vertically divided by sharp boundaries with non-turbulent regions.

Figure 1 shows a schematic energy spectrum for turbulence in the stratosphere. The spectrum is separated into the characteristic subranges which are based on the dominating physical processes. The transition between the inertial subrange and the viscous subrange defines the inner scale l_0. Typical values for l_0 in the stratosphere are in the range of centimeters. At very small scales (viscous subrange) the energy is dissipated into heat by viscosity. The aim of our measurements is to obtain this energy dissipation rate ε and thereby quantify the influence of turbulence on the stratosphere. Of particular interest is the relation of ε to atmospheric background profiles and specific geophysical situations like breaking gravity waves.

Remote sensing systems like radars, lidars and satellite-based sounders do not provide sufficient resolution to measure the turbulence spectrum down to the smallest scales or provide no signal at all in the middle stratosphere (e.g., Engler et al., 2005; Luce et al., 2002; Smalikho et al., 2005; Gurvich and Brekhovskikh, 2001; Sofieva et al., 2007). In-situ measurements are typically performed either below 15 km with aircrafts (e.g., Siebert et al., 2007) or above 60 km with sounding rockets (e.g., Lübken et al.,

AMTD
3, 3455–3487, 2010

2002). Thus in-situ high resolution balloon soundings still provide the only possibility for detailed observations of stratospheric turbulence. During the 1980s pioneering work has been done by J. Barat and coworkers with balloon-borne sensors (e.g., Barat, 1982; Barat et al., 1984; Dalaudier et al., 1989). Their measurements resolved scales down to some ten centimeters (i.e. within the inertial subrange). But exact turbulent energy dissipation rates can best be deduced by measurements covering the turbulent inner scale l_0 and part of the viscous subrange (Lübken, 1992). This implies that the spatial resolution must be at least 1 cm in the stratosphere. But those soundings are technically challenging and up to know stratospheric turbulence soundings are rare. In fact a sub-centimeter resolution has not been achieved yet.

We describe here an approach using a constant temperature anemometer (CTA) for high-resolution balloon borne wind soundings. The CTA allows us to measure wind fluctuations with a vertical resolution of 2.5 mm. Therewith for the first time it is possible to study the whole turbulence spectrum down to the viscous subrange in the stratosphere. Furthermore it is possible to obtain a detailed altitude profile of the energy dissipation rate. In the following section we present the instrument design of LITOS and the measurement principle of the CTA sensor. Since CTA systems have never been used before in the stratosphere, we performed laboratory tests to investigate the dynamic characteristics of the sensor. The test procedures and the results are described in Sect. 3. The payload has been launched successfully several times from our site at Kühlungsborn (Germany, 54° N, 12° E) and as part of the BEXUS 6 and BEXUS 8 payloads at Kiruna (Sweden, 67° N, 21° E). First results of the BEXUS 6 flight (8 October 2008) including energy dissipation rates are presented in Sect. 4.

2 Experimental method

Our balloon payload LITOS (Leibniz-Institute Turbulence Observations in the Stratosphere) consists of a CTA system plus telemetry, tracking hardware and housekeeping electronics. Additionally a radiosonde (Vaisala RS92) provides atmospheric background profiles of wind, temperature, humidity and pressure.

AMTD
3, 3455–3487, 2010

The measurement principle of CTA is based on convective cooling caused by the atmospheric air flow passing a heated thin wire (see Sect. 2.2). For our measurements we use a platinum plated tungsten wire (Type 55P03, Dantec Dynamics), which is 5 m in diameter and 1.25 mm long. The CTA signal output is A/D converted using a 16 bit ADC with 2000 samples per second resulting in a vertical resolution of 2.5 mm at 5 m/s ascent speed. In an improved version of LITOS the sampling rate has been increased to 8000 Hz, resulting in a ∼0.1 ms temporal resolution. (It should be noted here that the CTA system is generally specified up to 100 kHz.) We have integrated the CTA system into a styrofoam-box of 35 cm side length. To minimize the influences of the box on our measurements, the CTA sensor is placed ∼20 cm above the top of the payload (outside the shear layer around the box). The wire axis is vertical to achieve largest sensitivity for horizontal flow and less sensitivity for vertical flow due to the ascent of the balloon.

As the payload is not actively stabilized it may be affected by pendulum and rotational motions. While the pendulum motions have comparatively long periods of several seconds, the rotations may occur on different scales. In order to minimize the rotations we have attached a wind vane of about 40 cm diameter on a 50 cm boom to the payload box. Furthermore we have integrated a housekeeping system in the latest version of LITOS, to monitor the remaining rotations and accelerations. These measurements allow the identification and correction of any spurious maxima in the CTA spectra. LITOS can be used as one-way instrument if the telemetry conditions are sufficient (no obstruction by trees, houses or terrain). If a save recovery of the instrument is assured, the payload can be also used with on-board data storage. More details about the LITOS payload can be found in Gerding et al. (2009). In the next section we will explain the general principle of turbulence measurements with balloons. Section 2.2 includes the description of constant temperature anemometry with a special focus on our application.

AMTD
3, 3455–3487, 2010

2.1 Balloon measurement principle

Due to its large diameter the balloon is following the ambient wind field during the ascent phase (see Fig. 2). Ignoring pendulum motions for a moment, the payload at altitude z is also following the wind field in the height of the balloon at $z+h$. For a wind constant with altitude the effective flow observed in the height of the payload would be zero. Consequently any variation of the wind as observed by our sensor is the difference between the wind vectors in the balloon height $\boldsymbol{v}(z+h)$ and in the payload height $\boldsymbol{v}(z)$. Thus as a result we obtain an altitude profile of the wind differences $\Delta\boldsymbol{v}$. In the following we will use the term "wind" for the measured property instead of "wind difference" or "effective flow". Nevertheless it should be kept in mind that the absolute wind profile is only provided by the simultaneous radiosonde sounding (2 s resolution).

Finally, we want to point out that we also considered the balloon wake effect described by e.g., Barat et al. (1984). In order to assure that we measure pure atmospheric turbulence outside the balloon wake, the distance between the gondola and the balloon is much larger than the balloon diameter, namely 50–100 m.

2.2 Constant temperature anemometry

Constant temperature anemometry is a well known and widely used technique for flow measurements in gases and liquids in the laboratory. Their small size and light weight make CTA sensors particularly suitable for balloon-borne measurements. But so far they have never been used for stratospheric soundings. Regarding the general sensor behaviour several extensive studies were performed and have given theoretical and semi-empirical descriptions of the measured signal (e.g., Bruun, 1970; Bruun et al., 1988; van Dijk and Nieuwstadt, 2004). We refer to the literature for more details and only emphasize the main aspects with a special focus on our application.

CTA measurements are based on the convective cooling of a heated thin wire (here: 5 m diameter, 1.25 mm length) caused by atmospheric air flow passing the wire. The wire forms one leg of a Wheatstone bridge and is heated to a temperature of ~500 K.

AMTD
3, 3455–3487, 2010

The Wheatstone bridge is balanced by controlling the current through the wire so that the resistance – and hence temperature – is kept constant. Changes in the wind of the ambient atmosphere cause changes in the convective heat flow and consequently change the wire temperature, i.e. its resistance. Thus the resulting difference in the bridge voltage corresponds to the heat loss of the wire to the surrounding fluid, which in turn directly depends on the ambient flow velocity.

Generally, the heat from the wire is transferred to the surrounding fluid by radiation, free convection, the heat flow through the prongs and in particular by forced convection. The sum of these heat fluxes equals the supplied heat $\dot{Q}_E$, which is given by:

$$\dot{Q}_E = I^2 R = \frac{U^2}{R} = \dot{Q}_{rad} + \dot{Q}_{\text{freeconv}} + \dot{Q}_{\text{prongs}} + \dot{Q}_{\text{forcedconv}} \quad (1)$$

where U is the bridge voltage, R the wire resistance and I the electric current. Based on this relation the further determination of the heat loss imply the definition of the heat transfer coefficient α. The latter is expressed by the Nusselt number Nu, which is a dimensionless number describing the convective heat transfer from a surface. In the Appendix A we discuss the determination of the heat loss of the wire and the difficulty in the correct definition of Nu. Due to the complexity of the Nusselt number and the uncertainties in its determination we prefer the individual calibration of each wire. During the calibration procedure the wire is placed in a wind tunnel to adjust different laminar flow velocities. As a results a static calibration curve of the output voltages U as a function of the flow velocities v is obtained. Based on King (1914) the calibration data can be fitted by the modified King's law:

$$U^2 = A + Bv^n. \quad (2)$$

A and B are empirical calibration constants for each fluid. The exponent n depends slightly on the flow velocity. According to Jørgensen (2002) n=0.45 is a recommended starting value. By determining these calibration constants it is possible to convert the measured voltages to wind velocities.

AMTD
3, 3455–3487, 2010

The crucial point is that the calibration coefficients are only valid if the ambient conditions do not differ from those during the calibration. This concerns not only the atmospheric wind, but also the density, temperature and humidity (Cimbala and Park, 1990; Cardell, 1993; Durst et al., 1996; Hugo et al., 1999). Thus the calibration should be performed under ambient conditions similar to the conditions during the measurements. In our case, i.e. for stratospheric conditions, the density varies between 1.2 kg/m^{-3}, the (relative) wind velocities are up to 2 m/s and 1.2×10^{-3} kg/m^{-3} and the temperature decreases to ~200 K. The absolute humidity is well below 10%, thus the influence on our measurements is negligible (Durst et al., 1996).

We should point out here that for the analysis of turbulence it is not necessary to derive absolute wind velocity values from the CTA signal. Instead we make spectral analysis of the unscaled voltage signal to retrieve the spectral slope of the observed variations. Typically we analyse 4–20 s (i.e. 20–100 m) of data for a single spectrum. Within this period values for e.g. the temperature are sufficiently constant. From the spectral slope of the observed variations we deduce information about the stratospheric turbulence by calculating e.g. the energy dissipation rate. These numbers depend only on relative fluctuations and the particular length scale. However, no investigations for this wide pressure and temperature range have been done and the properties of the CTA sensor are completely unknown for stratospheric conditions. Therefore we performed laboratory tests within a climate and a vacuum chamber to check the response of the CTA on varying ambient conditions, i.e. temperature and pressure.

3 Laboratory experiments of CTA response

During all laboratory test procedures we used a small wind calibration unit for CTA sensors, which we placed into a climate and a vacuum chamber. While knowing the exact flow velocities we were able to set different values for the temperatures or pressure (i.e. density) of the flow passing the wire. Overall we made measurements for a velocity range of 3 m/s to 35 m/s at pressure levels between 50 hPa and 1000 hPa and for

AMTD
3, 3455–3487, 2010

a temperature range of 233–293 K. Due to technical limitations of the wind calibration unit we could not perform measurements below 3 m/s and below 50 hPa.

3.1 Temperature dependence of the CTA response

The heat transfer from the wire to the surrounding fluid is proportional to the temperature difference between the sensor and the fluid (see Appendix A, Eq. A2). From other experiments it is known that the CTA response is influenced by temperature variations (e.g., van Dijk and Nieuwstadt, 2004). For the correction of this temperature influence different methods are suggested in the literature (e.g., Bruun, 1995; Jørgensen, 2002). All correction methods are specified for mostly small temperature drifts and temperature ranges far away from stratospheric values. Therefore we investigated the CTA response within a climate chamber for the temperature range expected during a balloon flight (233–293 K). The results reveal a linear relation between the voltage signal of the CTA sensor and the temperature of the fluid. For our examined temperature range we found a maximum slope of 5 mV/K i.e. 0.23%/K. Due to this linear dependence we found no influence of the temperature on the sensitivity of the sensor. Nevertheless, before converting the measured voltage values to wind velocities, the temperature influence has to be corrected. The temperature correction method given by e.g., Jørgensen (2002) can be used (after adjusting the exponent mentioned therein).

3.2 Pressure dependence of the CTA response

In order to study the pressure influence on the sensor response we performed tests within a vacuum chamber. The temperature during the measurements changed less than 5 K and therefore does not affect the results.

Figure 3 shows the voltage signal for various velocities at different pressure levels. The thin lines represent the King's law fits (according to Eq. 2) for each pressure level. A direct pressure influence can easily be seen, as the slope decreases from 1000 hPa to e.g. 100 hPa. The question is now, whether this pressure influence will have an

AMTD
3, 3455–3487, 2010

impact on the sensitivity of the wire. In Fig. 4 we plotted the sensitivity $\Delta U/\Delta V$ as a function of velocity for the different pressure levels. Obviously the sensitivity decreases with decreasing pressure and this effect is most evident at lower velocities. Using these results of the vacuum chamber tests we demonstrate later in this paper, that the decreasing sensitivity of the sensor response has no impact on the spectral slopes of the turbulence measurements. Despite these findings we show in the Appendix B that there exists an upper limit for the use of CTA sensors in the atmosphere around ~1 hPa (~45 km). But during our measurements we are sufficiently below this limitation.

4 Balloon observations of turbulence

We have successfully launched our payload LITOS six times since December 2007. Four soundings have been carried out from our site at the Leibniz-Institute of Atmospheric Physics (IAP) in Kühlungsborn (Germany, 54° N/12° E). In addition, two soundings took place at the Esrange Space Center in Kiruna (Sweden, 67° N/21° E) as part of the BEXUS (Balloon EXperients for University Students) campaigns in 2008 and 2009. The main differences between the launches from Kühlungsborn and Kiruna are given in Table 1.

For the flights from Kühlungsborn we used rubber balloons, whereas the flights from Kiruna were performed with plastic balloons. The different type and size of the balloon leads to different movements in the vertical axis and in the horizontal plane. For further investigation of this subject, we have developed a housekeeping device including a 6-axis sensor, which measures the rotation and acceleration of the payload at a rate of 50 Hz and has been part of recent launches at Kühlungsborn. However, disturbing effects of rotation and acceleration are also considered in the data analysis (see below).

AMTD
3, 3455–3487, 2010

4.1 Timeseries of signal fluctuations

We will now show some initial results of LITOS measurements obtained during the BEXUS 6 flight from Kiruna. By removing a spline trend from the signal we eliminated low frequency disturbing effects (e.g. oscillation/rotation of the gondola). During this flight we observed many layers of turbulence. The vertical extent of these layers range from a few meters to some hundred meters, but normally do not exceed 500 m. As a typical example, Fig. 5 presents voltage fluctuations observed within such a turbulent layer (26 550–26 650 m).

For comparison and to emphasize that those fluctuations are caused by atmospheric turbulence and not by instrumental effects, we show an example of a non-turbulent region at 26 350–26 450 m (Fig. 6), i.e. 100 m below the turbulent layer presented in Fig. 5. The small remaining fluctuations are due to instrumental noise and do not exceed ∼0.002 V. These results demonstrate that the instrument works properly and is capable of detecting small scale turbulent fluctuations. Furthermore these results indicate that the turbulent regions are defined by sharp boundaries to the non-turbulent regions and therewith represent the layered structure of stratospheric turbulence. Those findings are consistent with earlier observations of e.g., Sato and Woodman (1982) and Barat (1982).

4.2 Spectral analysis of the BEXUS 6 timeseries

As explained before we obtain information about turbulence and turbulent energy dissipation rates from the spectral analysis of the measured relative voltage fluctuations. After removing a spline trend from the signal, we are using the Welch method to calculate power spectral density values (Welch, 1967). To reduce spectral leakage we apply a Hanning window function to the data before fitting. As a typical example, Fig. 7 presents the spectrum for the turbulent region shown in Fig. 5.

AMTD
3, 3455–3487, 2010

The spatial scales L are derived from $L=2\pi/k=v_b/f$ (k=wavenumber, f=frequency, v_b=balloon ascent velocity). A $m^{-5/3}$ slope is well identified between spatial scales of 8 m and 0.3 m as well as the transition to a m^{-7} slope below 0.1 m. The observed slopes nicely agree with the behavior for the inertial and viscous subrange of the turbulent spectrum expected from theory (see Fig. 1). The noise level of our instrument starts at a power spectral density value of $\sim 10^{-7}$ V/s. This demonstrates that our instrument has the required resolution and sensitivity to cover the inertial subrange and part of the viscous subrange of the turbulent spectrum. To our knowledge, these are the first in-situ measurements of turbulent spectra down to the viscous subrange in the stratosphere.

For comparison the spectrum of the non-turbulent region (Fig. 6) is shown in Fig. 8. In contrast to the turbulent spectrum, the slope does not follow the characteristic $m^{-5/3}$ behavior. The power spectral densities for scales smaller than 1 m are much lower than in the turbulent case and basically show instrumental noise. At very small spatial scales there are still some apparent irregularities (in both spectra) presumably due to electronic disturbances. But they do not hamper the spectral analysis.

4.3 Calculation of energy dissipation rate

From turbulent spectra it is possible to derive relevant geophysical parameters like turbulent energy dissipation rates (ε). Lübken (1992) and Lübken et al. (1993) described a method to determine ε from rocket borne measurements of density fluctuations. Their routine includes the fitting of a theoretical spectrum model to the measured turbulent spectrum and from the best fit they obtain the energy dissipation rate ε. The theoretical model refers back to Heisenberg (1948) and exhibits a $m^{-5/3}$ power law in the inertial subrange and a m^{-7} slope in the viscous subrange. Therewith it is possible to calculate the inner scale l_0, which characterises the transition between the inertial and the viscous subrange and basically determines the turbulent energy dissipation rate. The

AMTD
3, 3455–3487, 2010

relation is given by:

$$l_0 = 9.9 \left(\frac{\nu^3}{\varepsilon} \right)^{\frac{1}{4}} \quad (3)$$

with the kinematic viscosity ν. Further details of the procedure can be found in Lübken (1992) and Lübken et al. (1993). We have adapted this method to our data of relative voltage fluctuations. As an example the fitting result is plotted as a black line in Fig. 7. The theoretical fit nicely agrees with our measured spectrum and we obtain an inner scale l_0 of 9.8 cm and an energy dissipation rate ε of ~10 mW.

5 Discussion

The laboratory results shown in Sect. 3.2 reveal a non-linear dependence of the sensor sensitivity $\frac{\Delta U}{\Delta \nu}$ on pressure influences and furthermore a decreasing sensitivity of the sensor response with decreasing pressure. In addition the sensitivity also varies for different wind velocities (Fig. 4). In other words, the sensor sensitivity depends not only on pressure but also on the relative background wind. Since we measure relative wind velocities up to 2 m/s we are in the region with the largest influence of pressure and relative background wind (cf. Fig. 4). The question arises whether this could influence our turbulence measurements or rather the slope of the turbulence spectrum. Thus we exemplarily normalized the voltage fluctuations of Fig. 5 to the relative background wind measured simultaneously by the radiosonde. Due to the lower sampling rate (1 s) of the radiosonde data we interpolated the values to the sampling rate of the measured voltage fluctuations (0.5 ms) and therewith derived a value of the relative background wind for each value of the fluctuations. Based on the 100 hPa curve (Fig. 4) we then determined an individual correction factor for the sensitivity of each value along the sequence according to the relative wind at 26 550 m, i.e. the first value of the sequence. In fact by using the 100 hPa curve for this sequence we overestimated the

AMTD
3, 3455–3487, 2010

influence of the relative background wind: As can be seen from Fig. 4 the sensitivity change decreases with decreasing pressure, so at an altitude of 26 550 m (18 hPa) it is very likely that the sensitivity varies less compared to 100 hPa. Unfortunately, due to technical limitation of the wind calibration unit we could not proceed our measurements to pressure values below 100 hPa. (The 50 hPa values are omitted due to remaining ambiguities.)

Nevertheless, by applying the individual correction factor (obtained at 100 hPa) to the measured voltage fluctuations in the sequence we eliminated the influence of the background relative wind. Figure 9 shows the uncorrected signal (black) and the corrected signal (red) together with the relative wind measured by the radiosonde (blue). The influence of the relative background wind is obviously rather small. Furthermore the spectra of the corrected and uncorrected signals are quite similar (Fig. 10). Here the largest deviations appear at larger spatial scales and decrease down to smaller scales. The resulting energy dissipation rates for the corrected and uncorrected spectra deviate by ~2%. Thus it is well justified to use the uncorrected signal for the determination of turbulence parameters.

6 Summary and conclusions

In this paper we presented first results of a new compact balloon-borne instrument called LITOS (Leibniz-Institute Turbulence Observations in the Stratosphere). LITOS measures wind fluctuations in the stratosphere with very high vertical resolution (2.5 mm). The first flight took place on 12 December 2007 and the instrument has been improved further since. A constant temperature anemometer (CTA) is the main part of the balloon payload LITOS, which has a total weight of less than 5 kg and can be launched from any radiosonde station.

There is very little knowledge in the literature about CTA measurements at low pressures and we have performed our own laboratory studies within a vacuum chamber. The studies show a decreasing sensitivity with decreasing pressure. Nevertheless we have shown that for our purpose the CTA technique is well suitable. The main goal

AMTD
3, 3455–3487, 2010

of our measurements is to obtain geophysical parameters like the turbulent energy dissipation rate. These numbers depend on relative fluctuations and the particular length scale only, thus we can deduce information about the stratospheric turbulence from the unscaled voltage signal.

We have shown results of the BEXUS 6 flight launched from Kiruna on 8 October 2008, where we observed several turbulent layers with a vertical extent ranging from a few meters to some hundred meters. There are sharp boundaries between turbulent and quiet regions. Our observations confirm the findings of e.g., Barat (1982). The measurement resolution has been strongly improved compared to the soundings from Barat and coworkers in 1980s. Due to the unprecedented resolution of our measurements, we are able to measure the turbulent spectrum in the stratosphere down to viscous subrange. To our knowledge this was not done before. The turbulent spectra of the measured voltage fluctuations nicely agree with the theoretically expected behavior of turbulence in the inertial and viscous subrange. By fitting a spectral model to the spectrum of voltage fluctuations we determine the inner scale and therewith the energy dissipation rate. For the presented example of a turbulence spectrum measured by LITOS, the fitting procedure yields an energy dissipation rate of 10 mW and a inner scale of 9.8 cm. The value of ε deviates by a factor of up to 100 from earlier indirect measurements. Future flights are planned to get a "climatology" of stratospheric turbulence and to characterise selected wave breaking situations.

Appendix A

Theoretical determination of the heat transfer

The heat transfer from the wire to the surrounding fluid is a sum of the heat flow due to forced convection, free convection, radiative cooling and the heat flow through the prongs:

$$\dot{Q}_E = \dot{Q}_{\text{forcedconv}} + \dot{Q}_{\text{freeconv}} + \dot{Q}_{\text{rad}} + \dot{Q}_{\text{prongs}}. \quad \text{(A1)}$$

AMTD
3, 3455–3487, 2010

Due to the small size of the heated wire the term of radiative cooling $\dot{Q}_{rad}$ is considerably smaller than the heat which is transferred from the sensor by forced convection (Durst, 2008). Consequently the heat loss resulting from radiation can be neglected.

According to Collis and Williams (1959) the term of free convection $\dot{Q}_{freeconv}$ can be omitted, if

$$Re > Gr^{1/3} \tag{A2}$$

with the Reynolds number Re

$$Re = \frac{v\, d_w}{\nu} \tag{A3}$$

(v=flow velocity, d=wire diameter and ν=kinematic viscosity of the fluid) and the Grashof number Gr

$$Gr = g(T_w - T_a)\, \frac{d_w^3}{\nu^2\, T_a}, \tag{A4}$$

(g is the gravitation acceleration, T_w the wire temperature and T_a the temperature of the ambient fluid). To verify Eq. (A2) we calculated the Grashof number and the Reynolds number using typical data from our soundings. Throughout the whole ascent phase Re is much larger than $Gr^{1/3}$ and therefore we can omit the free convection term in the heat transfer Eq. (A1). To minimize the (artificial) heat flow from the tungsten wire to the prongs ($\dot{Q}_{prongs}$), the wire has gold-plated ends connecting it with the wire prongs. Nevertheless for typical CTA applications the heat loss to the prongs amounts to about 10–20% of the total heat loss from the sensor (Durst, 2008). Thus the heat flow through the prongs is considered to be proportional to the forced convective flow and Eq. (A1) simplifies to

$$\dot{Q}_E \approx c \cdot \dot{Q}_{forcedconv} \tag{A5}$$

with c=const.

AMTD
3, 3455–3487, 2010

Finally according to Eq. (1) we get

$$U^2 = c\, R\, \dot{Q}_{\text{forcedconv}}. \tag{A6}$$

Thus the measured voltage signal is directly related to the heat loss through forced convection. The latter is defined as:

$$\dot{Q}_{\text{forcedconv}} = \alpha\, \pi\, l_{\text{w}}\, d_{\text{w}}\, (T_{\text{w}} - T_{\text{a}}), \tag{A7}$$

where α is the heat-transfer coefficient and l_{w} the wire length. The heat-transfer coefficient is given by

$$\alpha = \frac{Nu\, k}{d_{\text{w}}} \tag{A8}$$

with Nu=Nusselt number and k=heat conduction of the fluid. By inserting Eqs. (1), (A7) and (A8) in Eq. (A5) one obtains for the measured voltage

$$U^2 = c\, Nu\, k\, \pi\, l_{\text{w}}\, R\, (T_{\text{w}} - T_{\text{a}}). \tag{A9}$$

The Nusselt number is defined as

$$Nu = Nu(Re, Gr, Kn, Pr, Ma, l/d, \delta T, \ldots). \tag{A10}$$

For further examination Nu has to be determined individually for every used wire and the flow properties described by e.g. Re, Gr, the Knudsen number Kn, the Prandtl number Pr and the Mach number Ma. There exist several approaches in the literature for the empirical estimation of the Nusselt number for specific flow conditions (e.g., Collis and Williams, 1959; Cimbala and Park, 1990; Durst et al., 1996). The advantage of those formulations of Nu is that the heat loss from the wire and the dependence on the flow velocity can be obtained without calibration. However, a precise knowledge of all influencing parameters can not be provided with sufficient accuracy. For example, parameters of the wire (i.e. effective length and diameter) are not available with the required precision due to the complicated process of the wire manufacturing. Hence, the individual calibration method is preferentially used.

AMTD
3, 3455–3487, 2010

Appendix B

Knudsen number

Figure 4 rises the questions whether the sensor sensitivity decreases further at pressures below 100 hPa and whether there is a lower pressure limit for CTA soundings.

Furthermore the heat transfer equation for the interpretation of the CTA signal (as explained in Appendix A) requires continuum flow conditions. We therefore have to investigate the flow conditions during the balloon ascent phase. With the help of the Knudsen number it is possible to determine whether continuum flow approximations are applicable or not. The Knudsen number Kn is defined as the dimensionless ratio of the mean free path λ to a characteristic length scale, in our case the wire diameter d,

$$Kn = \lambda / d . \tag{B1}$$

The flow regime can be divided into the continuum flow ($Kn<10^{-2}$), the slip flow regime ($10^{-2}>Kn<10^{-1}$) and the free molecular flow for $Kn>10$ (e.g., Devienne, 1965). Figure 11 shows the Knudsen number for our vacuum tests and for the BEXUS 6 flight. Typically CTA measurements are performed in the slip flow regime, where continuum flow equations are still appropriate. With decreasing pressure the heat transfer to the surrounding medium by convection decreases. Finally in the free molecular flow continuum approximations are no longer applicable. Therewith a lower pressure limit for CTA soundings can be estimated when $Kn>10$, i.e. at ~1 hPa (~45 km). As can be seen from Fig. 11 in our case the Knudsen number is well below 10, i.e. our measurements do not proceed to the free molecular flow. Hence, for our purpose CTA is well suitable, since the measurement principle itself is valid.

AMTD
3, 3455–3487, 2010

Acknowledgements. We acknowledge the support by the Leibniz graduate school ILWAO, jointly funded by the MBWK (for the government of Mecklenburg-Vorpommern) and the BMBF (for the German federal government). Additionally we thank SNSB (Swedish National Space Board) and DLR (German Aerospace Center) for the possibility to be part of the BEXUS 6 payload. We thank our colleague Torsten Köpnick (IAP) for his support in hardware development.

References

Barat, J.: Some characteristics of clear air turbulence in the middle stratosphere, J. Atmos. Sci., 39, 2553–2564, 1982. 3457, 3458, 3465, 3469

Barat, J., Cot, C., and Sidi, C.: On the measurement of the turbulence dissipation rate from rising balloons, J. Atmos. Oceanic Technol., 1, 270–275, 1984. 3458, 3460

Bruun, H.: Hot-Wire Anemometry – Principles and Signal Analysis, Oxford Science Publication, Oxford, 1995. 3463

Bruun, H. H.: Interpretation of a hot wire signal using a universal calibration law, J. Phys. E: Sci. Instrum., 4, 225–231, 1970. 3460

Bruun, H. H., Khan, M. A., Al-Kayiem, H. H., and Fardad, A. A.: Velocity calibration relationships for hot-wire anemometry, J. Phys. E: Sci. Instrum., 21, 225–232, 1988. 3460

Cardell, G.: A note on the temperature-dependent hot-wire calibration method of Cimbala and Park, Exp. Fluids, 14, 283–285, 1993. 3462

Cimbala, J. M. and Park, W. J.: A direct hot-wire calibration technique to account for ambient temperature drift in incompressible flow, Exp. Fluids, 8, 299–300, 1990. 3462, 3471

Collis, D. C. and Williams, J.: Two-dimensional convection from heated wires at low Reynolds numbers, J. Fluid Mech., 6, 357–389, 1959. 3470, 3471

Dalaudier, F., Crochet, M., and Sidi, C.: Direct comparison between in situ and radar measurements of temperature fluctuation spectra: a puzzling result, Radio Sci., 24, 311–324, 1989. 3458

Devienne, F. M.: Low-density heat transfer, Advances in Heat Transfer, 2, 271–356, 1965. 3472

Durst, F.: An Introduction to the Theory of Fluid Flows, Springer-Verlag, Berlin, 2008. 3470

Durst, F., Noppenberger, S., Sill, M., and Venzke, H.: Influence of humidity on hot-wire measurements, Meas. Sci. Technol., 7, 1517–1528, 1996. 3462, 3471

AMTD

3, 3455–3487, 2010

Engler, N., Latteck, R., Strelnikov, B., Singer, W., and Rapp, M.: Turbulent energy dissipation rates observed by Doppler MST Radar and by rocket-borne instruments during the MIDAS/MaCWAVE campaign 2002, Ann. Geophys., 23, 1147–1156, doi:10.5194/angeo-23-1147-2005, 2005. 3457

Gerding, M., Theuerkauf, A., Suminska, O., Köpnick, T., and Lübken, F.-J.: Balloon-borne hot wire anemometer for stratospheric turbulence soundings, Proceedings of the 19th ESA Symposium on European Rocket and Balloon Programmes and Related Research, SP-671, 175–180, 2009. 3459

Gurvich, A. S. and Brekhovskikh, V. L.: Study of the turbulence and inner waves in the stratosphere based on the observations of stellar scintillations from space: a model of scintillation spectra, Waves Random Complex, 11, 163–181, 2001. 3457

Heisenberg, W.: Zur statistischen Theorie der Turbulenz, Z. Phys., 124, 628–657, 1948 (in German). 3466

Hocking, W.: Turbulence in the region 80–120 km, Adv. Space Res., 10 (12), 153–161, 1990. 3457

Hugo, R. J., Nowlin, S. R., Eaton, F. D., Bishop, K. P., and McCrae, K. A.: Hot-wire calibration in a non-isothermal incompressible pressure variant flow, Proceedings of the SPIE symposium "Airborne Laser Advanced Technlogy II", 3706, 11–23, 1999. 3462

Jørgensen, F.: How to measure turbulence with hot-wire anemometers a practical guide, Publication 9040U6151, Dantec Dynamics A/S, Skovlunde, Denmark, 2002. 3461, 3463

King, J. V.: On the convection of heat from a small cylinder in a stream of fluid: determination of the convection constant of small platinum wires with application to hot-wire anemometry, Phil. Trans. R. Soc., 214, 373–432, 1914. 3461

Lilly, D. E., Waco, D. E., and Adelfang, S. I.: Stratospheric mixing from high-altitude turbulence measurements, J. Appl. Meteor., 13, 488–493, 1974. 3457

Lübken, F., Rapp, M., and Hoffmann, P.: Neutral air turbulence and temperatures in the vicinity of polar mesosphere summer echoes, J. Geophys. Res., 107, 4273–4277, 2002. 3457

Lübken, F.-J.: On the extraction of turbulent parameters from atmospheric density fluctuations, J. Geophys. Res., 97, 20385–20395, 1992. 3457, 3458, 3466, 3467

Lübken, F.-J., Hillert, W., Lehmacher, G., and von Zahn, U.: Experiments revealing small impact of turbulence on the energy budget of the mesosphere and lower thermosphere, J. Geophys. Res., 98, 20369–20384, 1993. 3466, 3467

AMTD
3, 3455–3487, 2010

Luce, H., Fukao, S., Dalaudier, F., and Crochet, M.: Strong mixing events observed near the tropopause with the MU radar and high resolution balloon techniques, J. Atmos. Sci., 59, 2885–2896, 2002. 3457

Rauthe, M., Gerding, M., and Lübken, F.-J.: Seasonal changes in gravity wave activity measured by lidars at mid-latitudes, Atmos. Chem. Phys., 8, 6775–6787, doi:10.5194/acp-8-6775-2008, 2008. 3457

Sato, T. and Woodman, R.: Fine altitude resolution observations of stratospheric turbulent layers by the Arecibo 430 MHz radar, J. Atmos. Sci., 39, 2546–2552, 1982. 3457, 3465

Siebert, H., Lehmann, K., and Shaw, R.: On the use of hot-wire anemometers for turbulence measurements in clouds, J. Atmos. Oceanic Technol., 24, 980–993, 2007. 3457

Smalikho, I., Kopp, F., and Rahm, S.: Measurement of atmospheric turbulence by 2-μ Doppler lidar, J. Atmos. Oceanic Technol., 22, 1733–1747, 2005. 3457

Sofieva, V. F., Gurvich, A. S., Dalaudier, F., and Kan, V.: Reconstruction of internal gravity wave and turbulence parameters in the stratosphere using GOMOS scintillation measurements, J. Geophys. Res., 112, D12113, doi:10.1029/2006JD007483, 2007. 3457

van Dijk, A. and Nieuwstadt, F. T. M.: The calibration of (multi-) hot – wire probes: 1. temperature calibration, Exp. Fluids, 36, 540–549, 2004. 3460, 3463

Welch, P. D.: The Use of Fast Fourier Transform for the Estimation of Power Spectra: A Method Based on Time Averaging Over Short, Modified Periodograms, IEEE T. Acoust. Speech, AU-15, 70–73, 1967. 3465

AMTD

3, 3455–3487, 2010

Table 1. Overview of launched LITOS payloads.

launch site	Kühlungsborn (54° N, 12° E)	Kiruna (67° N, 21° E)
balloon size	1200–3000 g	10 000 m^3/12 000 m^3
balloon type	rubber	plastic
gondola weight	5 kg	121 kg/140 kg
distance balloon-gondola	100 m	60 m
max. altitude	35 km	29 km

AMTD
3, 3455–3487, 2010

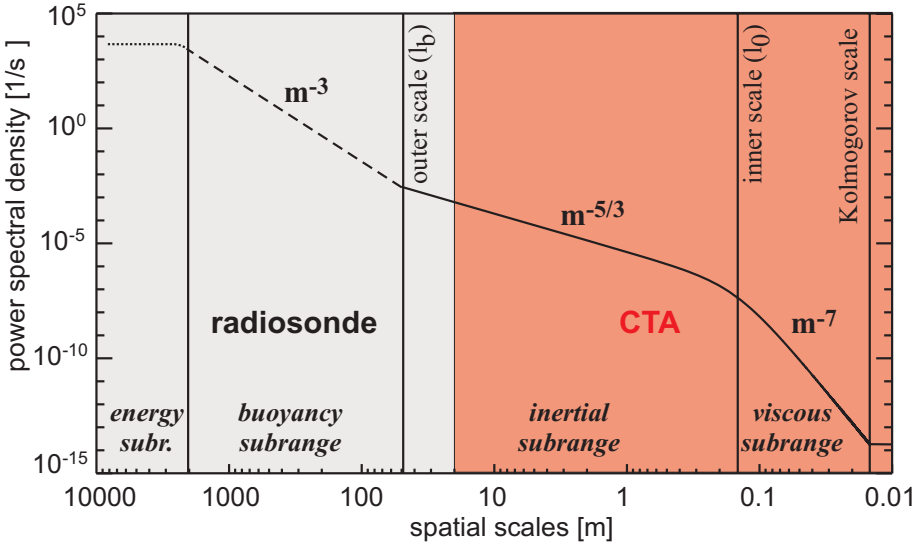

Fig. 1. Theoretical turbulent spectrum with typical values of the inner scale (l_0=0.146 m) and the energy dissipation rate (ε=0.001 W/kg) for 20 km altitude. In contrast to a normal radiosonde the constant temperature anemometer (CTA) enables the measurement of the spectrum down to the viscous subrange.

AMTD
3, 3455–3487, 2010

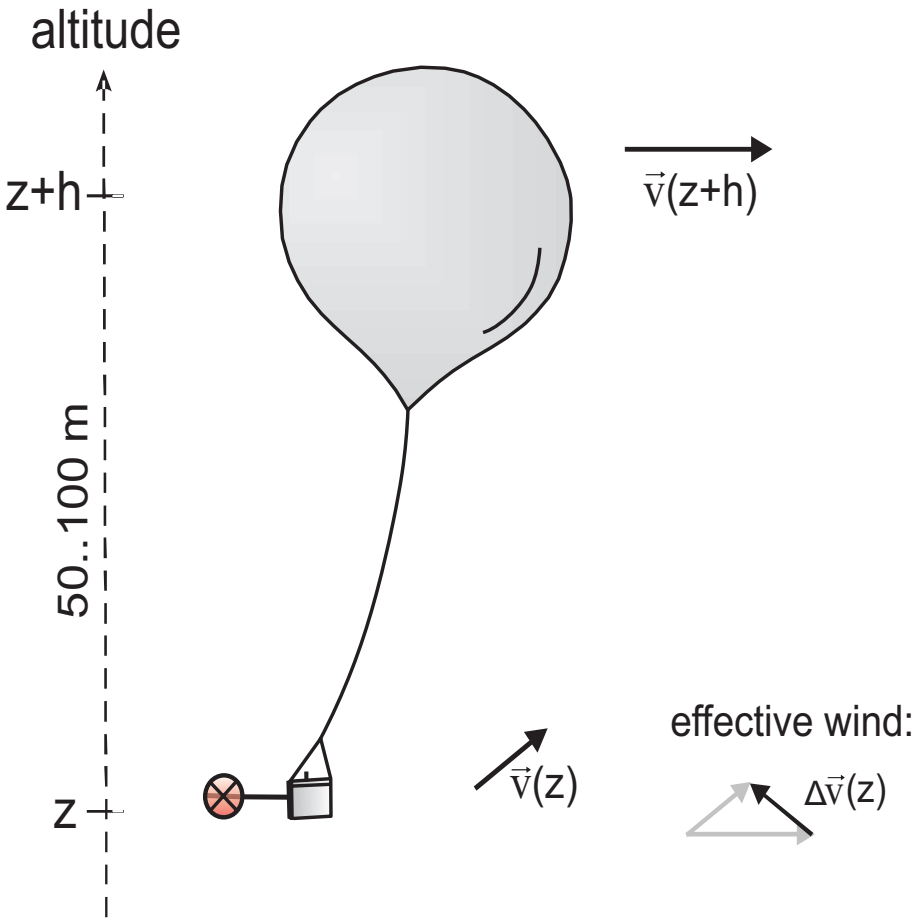

Fig. 2. Schematic drawing of the principle of balloon borne wind turbulence soundings.

AMTD
3, 3455–3487, 2010

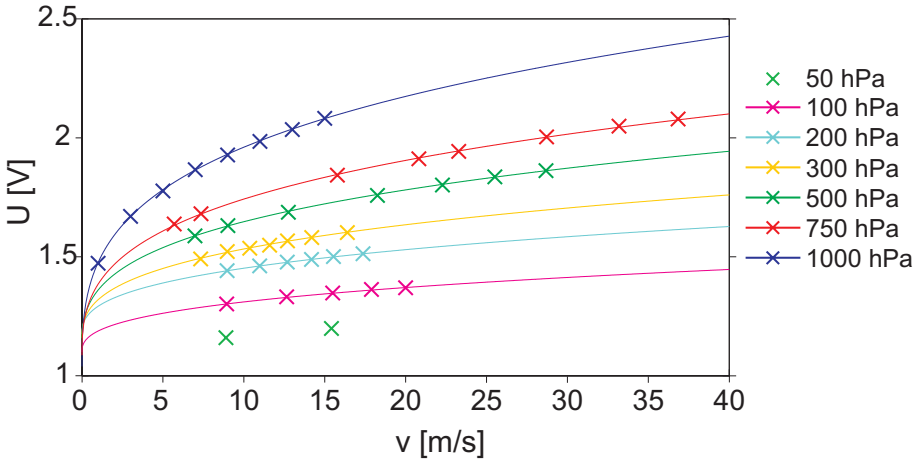

Fig. 3. King's law fits (thin lines) of the CTA signals (data points) for different pressure levels as measured within a vacuum chamber. For 50 hPa only two points are obtained. Thus the King's law fit is omitted due to remaining ambiguities.

AMTD
3, 3455–3487, 2010

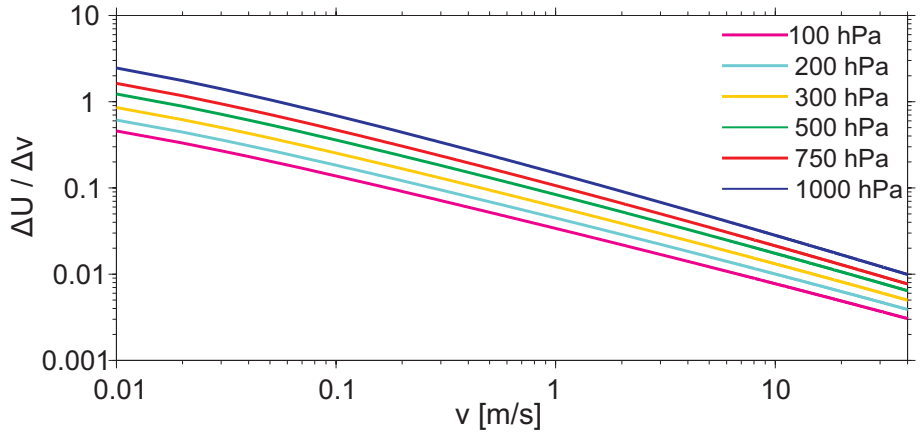

Fig. 4. Sensitivity of the CTA signal against wind velocity for different pressure levels as measured within a vacuum chamber.

AMTD
3, 3455–3487, 2010

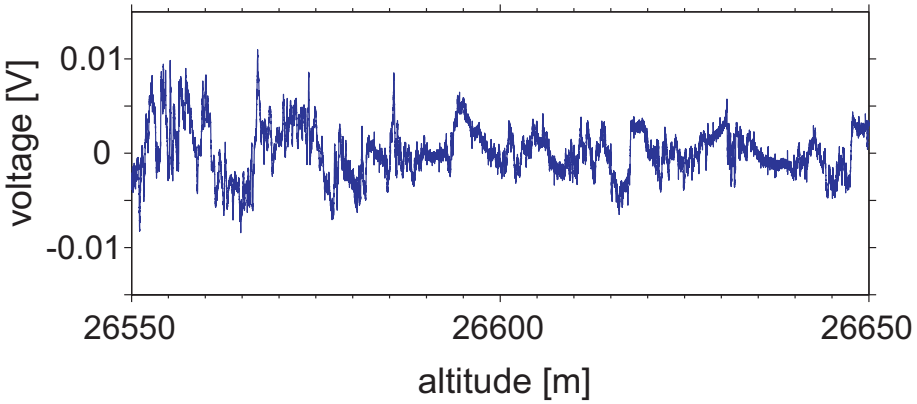

Fig. 5. Time record (converted to altitude) of the measured voltage fluctuations in a turbulent region during the BEXUS 6 flight on 8 October 2008.

AMTD
3, 3455–3487, 2010

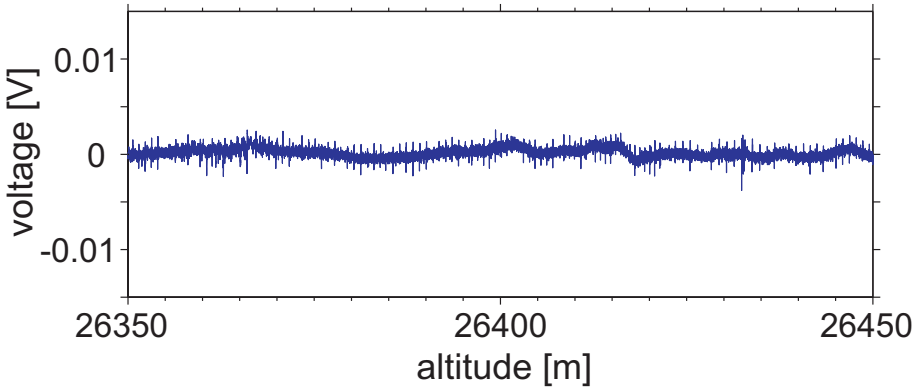

Fig. 6. Time record (converted to altitude) of the measured voltage fluctuations in a non-turbulent region during the BEXUS 6 flight on 8 October 2008.

AMTD
3, 3455–3487, 2010

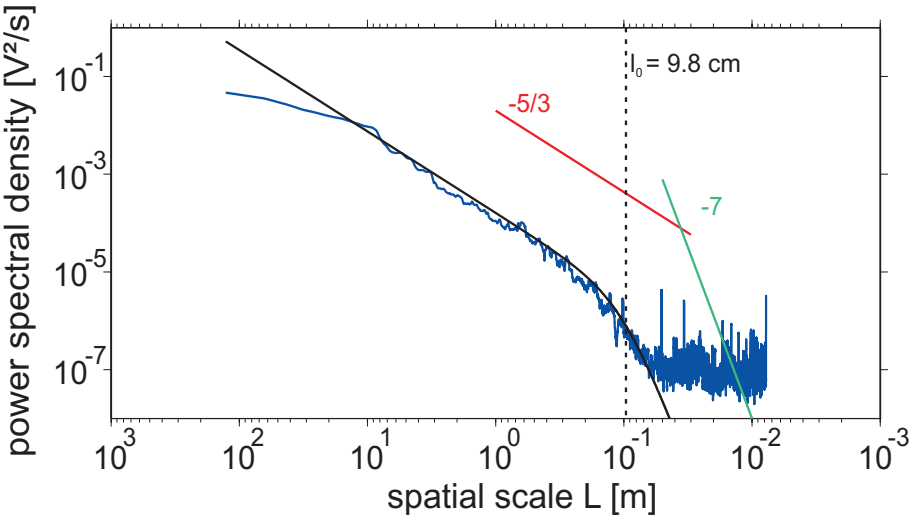

Fig. 7. Power spectrum of the voltage fluctuations for 26 550–26 650 m altitude together with the best model fit. Values of 9.8 cm for the inner scale l_0 and 10 mW for the energy dissipation rate ε are derived from the fit routine. The kinematic viscosity is $\nu = 4.7 \times 10^{-4}$ m^2/s.

AMTD
3, 3455–3487, 2010

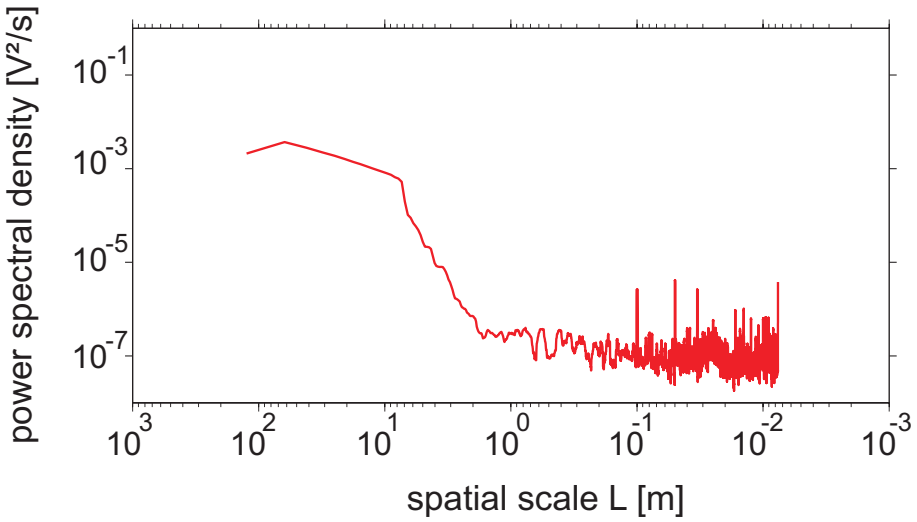

Fig. 8. Calculated Fourier spectrum of the voltage fluctuations for the non-turbulent region (26 350–26 450 m) from Fig. 6.

AMTD
3, 3455–3487, 2010

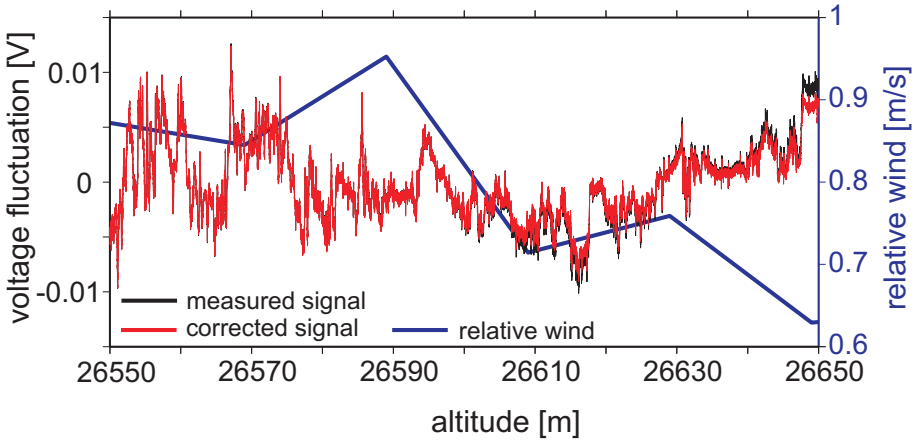

Fig. 9. Measured voltage fluctuations for the same altitude region as in Fig. 5. The black line shows the measured fluctuations and the red line shows the fluctuation corrected for changes of background relative wind. The blue line presents the relative wind measured by radiosonde (used for the correction).

AMTD
3, 3455–3487, 2010

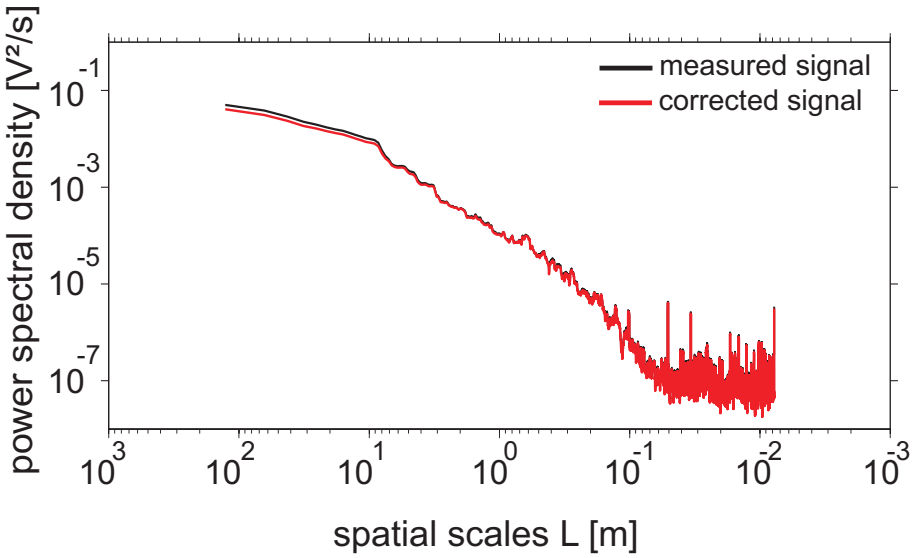

Fig. 10. Spectra of the corrected (red) and uncorrected (black) voltage fluctuations from Fig. 9.

AMTD
3, 3455–3487, 2010

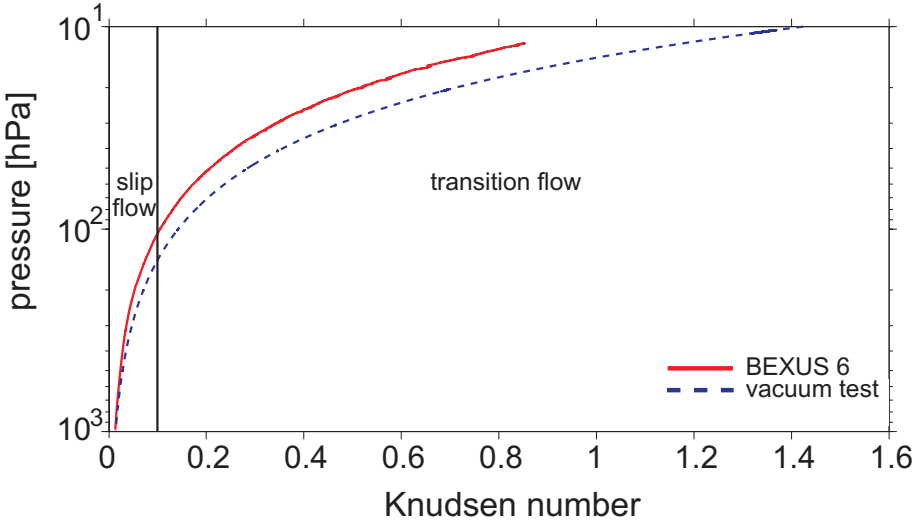

Fig. 11. Knudsen number for the vacuum test and for the BEXUS 6 flight.

AMTD
3, 3455–3487, 2010